ADVANCED MATERIALS INTERFACES

Supporting Information

for *Adv. Mater. Interfaces,* DOI: 10.1002/admi.202200575

Atomic Layer Engineering of Aluminum-Doped Zinc Oxide Films for Efficient and Stable Perovskite Solar Cells

Joanna Kruszyńska, Jakub Ostapko, Veysel Ozkaya, Belkis Surucu, Oliwia Szawcow, Kostiantyn Nikiforow, Marcin Hołdyński, Mohammad Mahdi Tavakoli, Pankaj Yadav, Małgorzata Kot, Grzegorz Piotr Kołodziej, Mateusz Wlazło, Soumitra Satapathi, Seckin Akin, and Daniel Prochowicz**

Supporting Information

Atomic Layer Engineering of Aluminum doped Zinc Oxide Films for Efficient and Stable Perovskite Solar Cells

J. Kruszyńska, J. Ostapko, V. Ozkaya, B. Surucu, O. Szawcow, K. Nikiforow, M. Hołdyński, M. M. Tavakoli, P. Yadav, M. Kot, G. P. Kołodziej, M. Wlazło, S. Satapathi, S. Akin, D. Prochowicz**

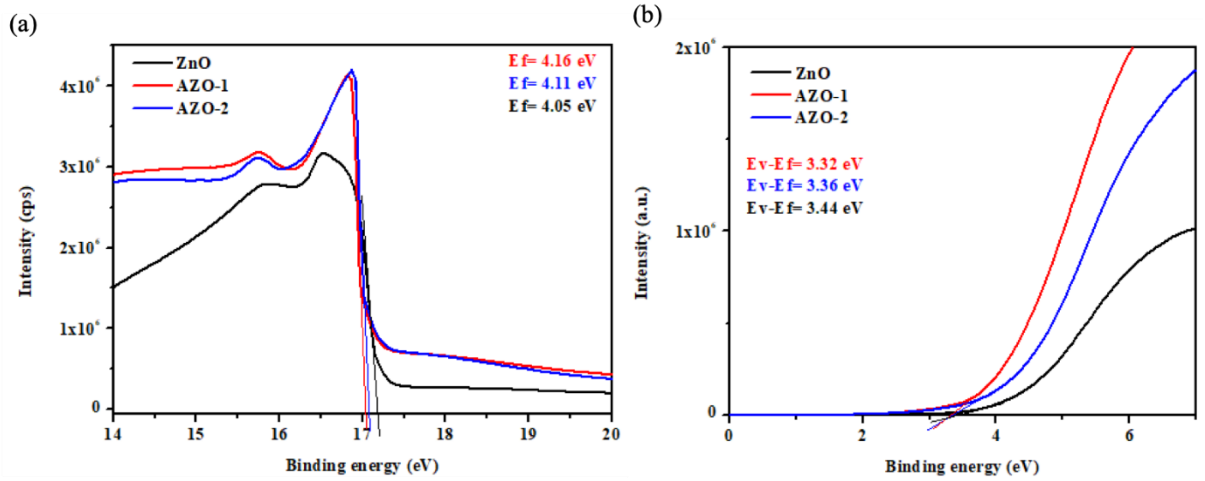

Figure S1. UPS measurement of ZnO, AZO-1, and AZO-2 films; (a) Fermi levels and (b) gap energy between valence band and Fermi level estimation.

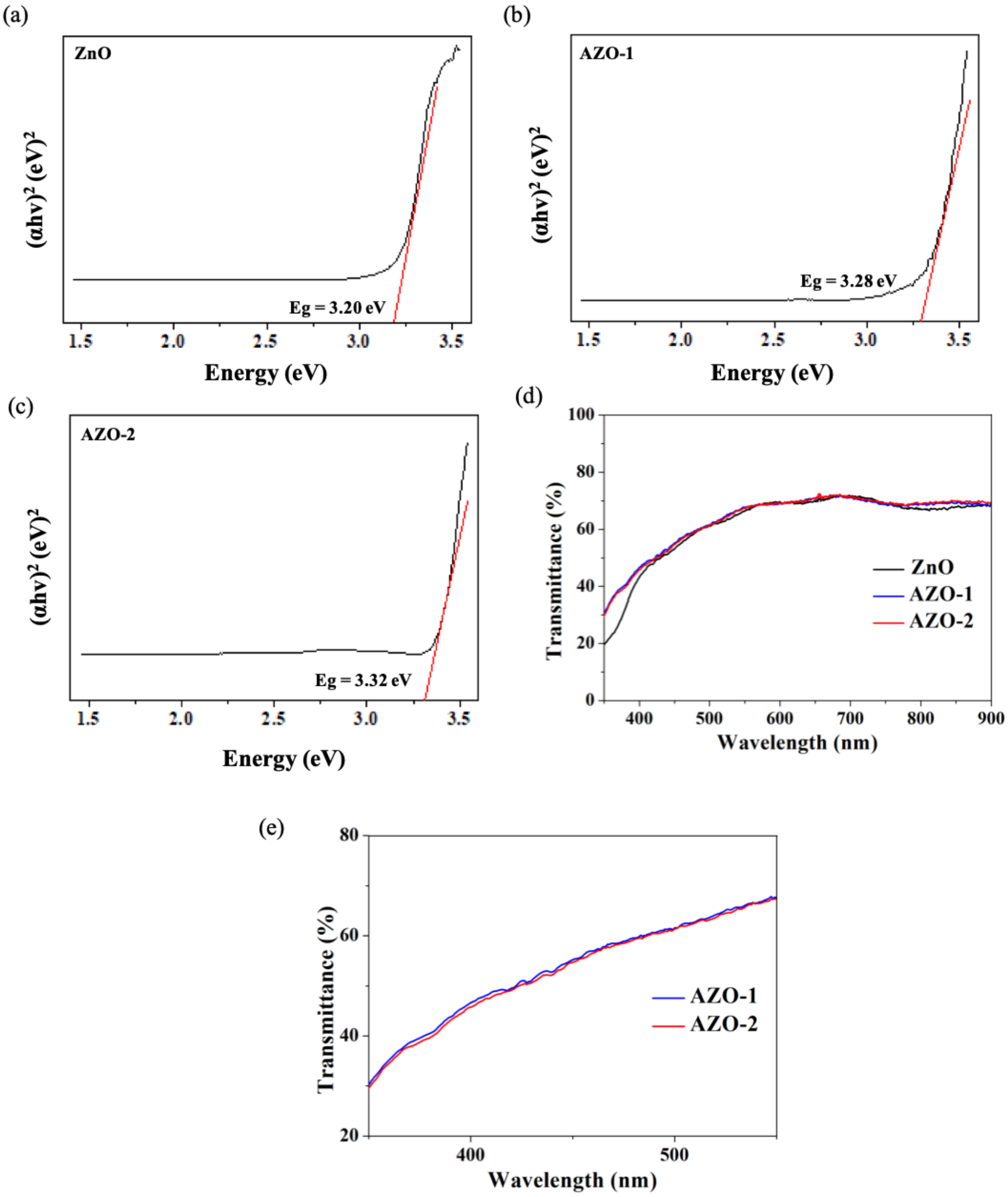

Figure S2. Bandgap calculation of (a) ZnO; (b) AZO-1 and (c) AZO-2 films. (d) Transmittance spectra of the investigated films and (e) magnification zoom on the transmittance spectra of AZO-1 and AZO-2.

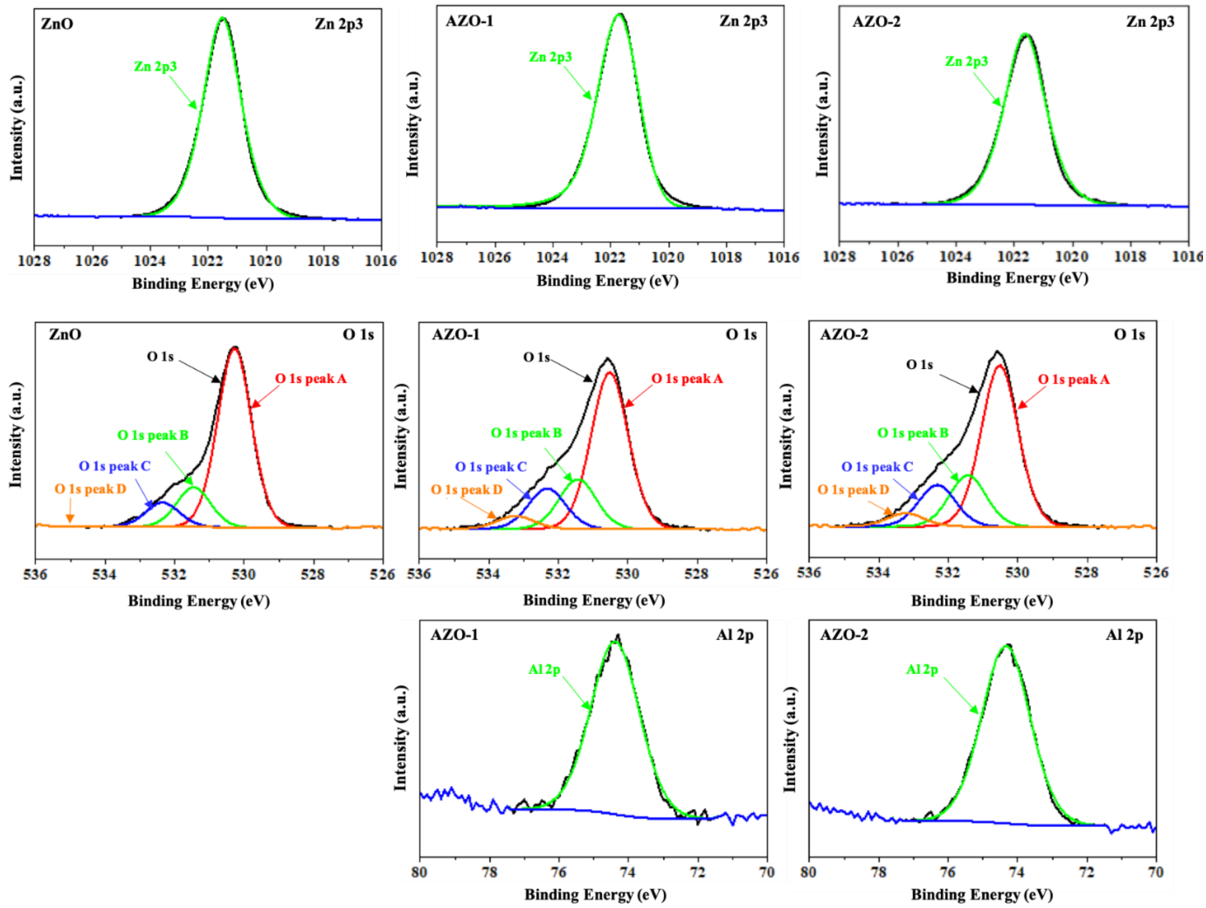

Figure S3. XPS spectra of ZnO, AZO, and AZO-AlO$_x$ films.

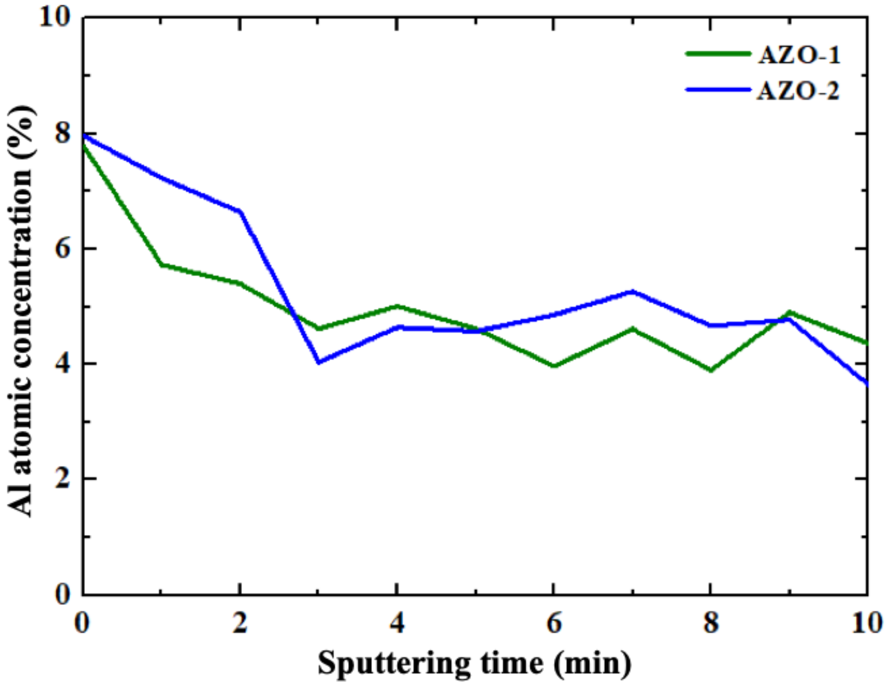

Figure S4. Concentration–depth profile of the aluminum in AZO samples obtained using Ar$^+$ ion sputtering.

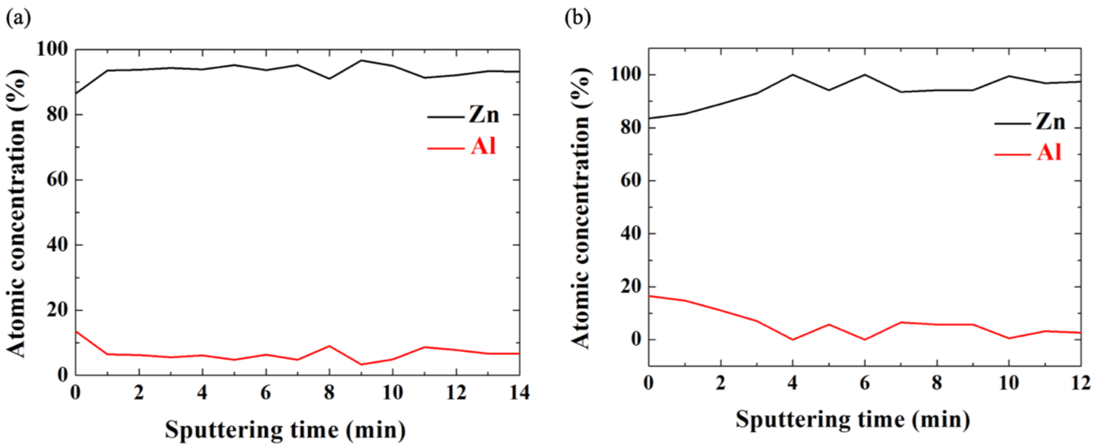

Figure S5. Average ratio of Al to Zn in bulk material of (a) AZO-1 and (b) AZO-2 obtained from XPS profiling.

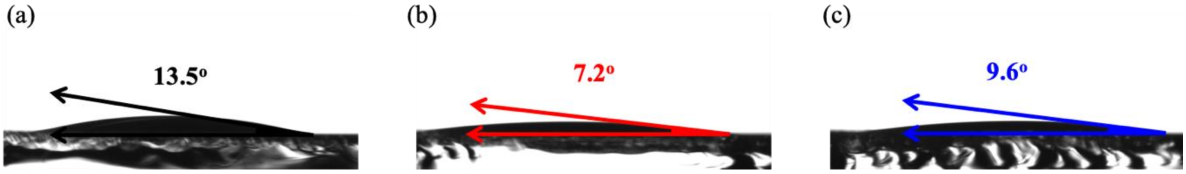

Figure S6. Water contact angle measurements on (a) ZnO; (b) AZO-1 and (c) AZO-2 ETLs.

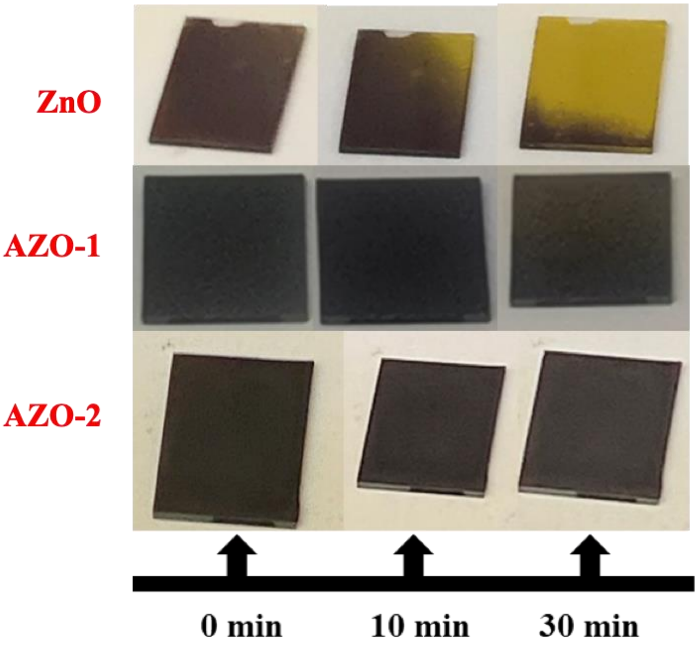

Figure S7. The optical images of perovskite films deposited on different ETLs and annealed at 100 °C for 10 and 30 minutes.

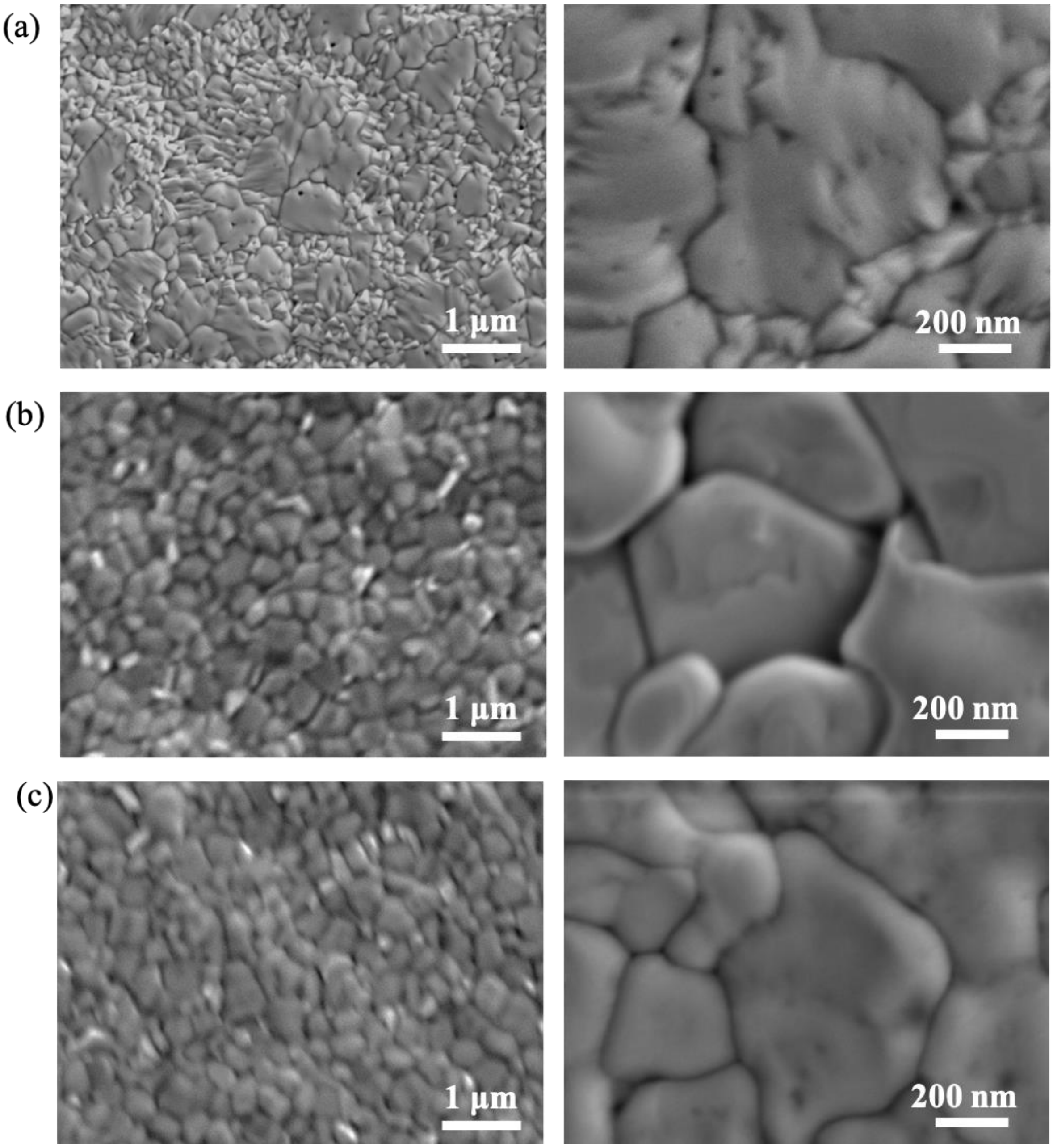

Figure S8. Top-view SEM images of perovskite films at different magnifications treated with 100 °C for 10 min and deposited on (a) ZnO, (b) AZO-1, and (c) AZO-2 films.

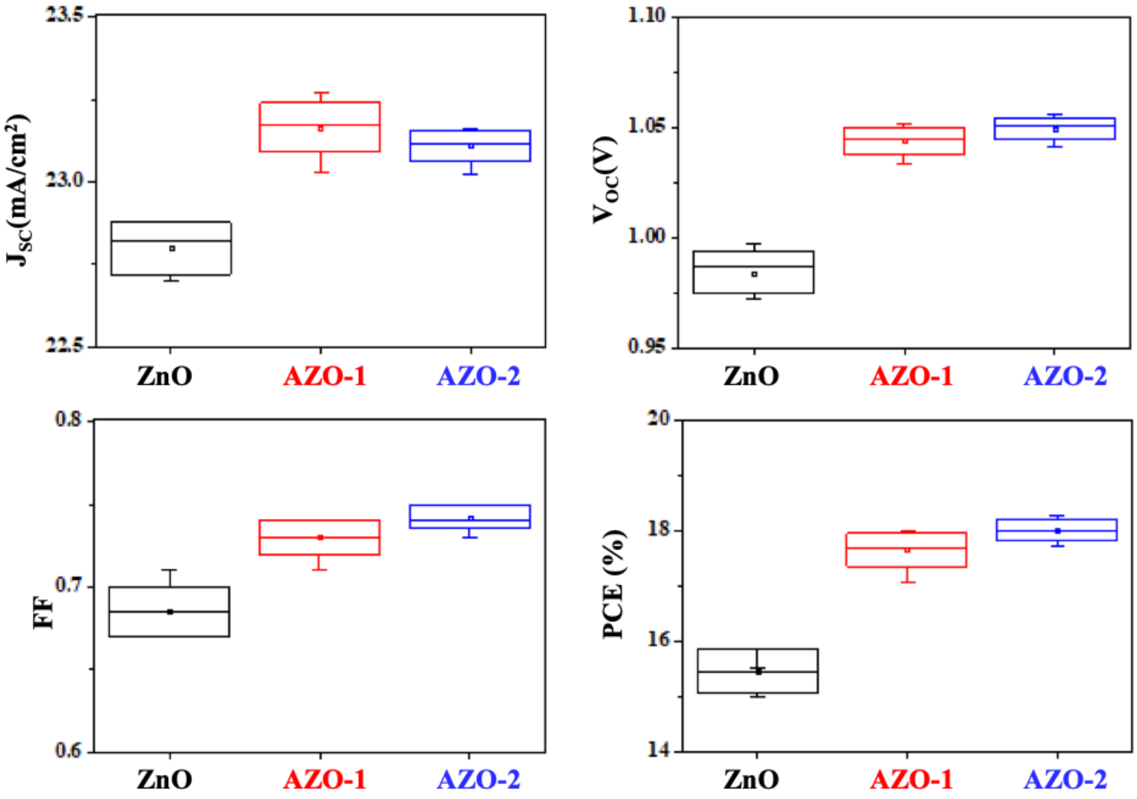

Figure S9. Statistic histogram of PCE, J_{SC}, V_{OC}, and FF from the collected cells based on ZnO, AZO-1and AZO-2 ETLs.

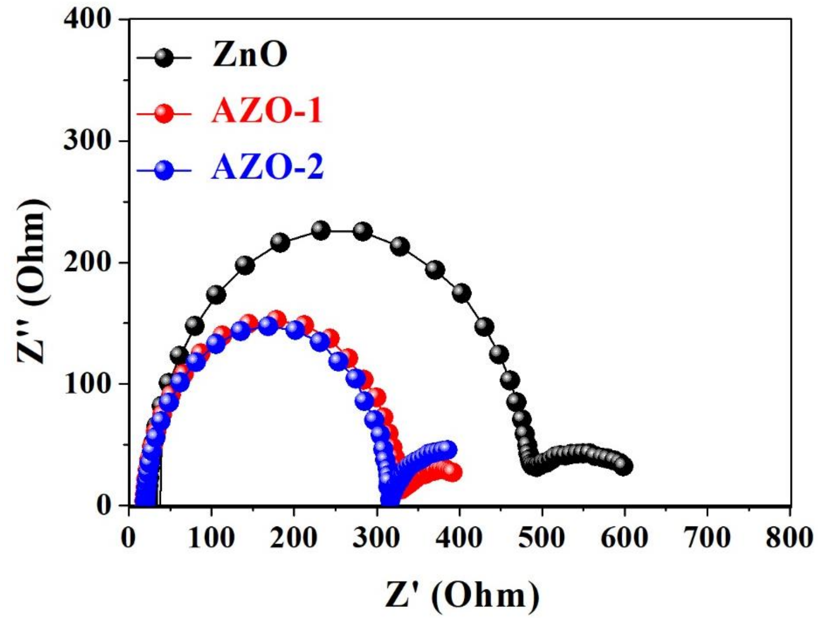

Figure S10. Dark EIS measurements measured near the V_{OC} for devices based on ZnO, AZO-1 and AZO-2 ETLs.

Table S1. Calculation of GPC for AZO deposition process.

Cycles	**Number of macrocycles**	**d, nm**	**GPC, nm/cycle**
143×(19×ZnO+1×AlO$_x$)+19×ZnO+1×WAT	144	450	3.13
57×(19×ZnO+1×AlO$_x$)+19×ZnO+1×WAT	58	174	3.00
24×(19×ZnO+1×AlO$_x$)+19×ZnO+1×WAT	25	75	3.00
115×(19×ZnO+1×AlO$_x$)+19×ZnO+1×WAT	116	390	3.36
80×(19×ZnO+1×AlO$_x$)+19×ZnO+1×WAT	81	256	3.16
		Average GPC :	3.12

Table S2. Calculation of GPC for ZnO deposition process.

Cycles	**Number of cycles**	**d, nm**	**GPC, nm/cycle**
156×ZnO+1×WAT	156	25	0.160
289×ZnO+1×WAT	289	48	0.166
434×ZnO+1×WAT	434	75	0.173
585×ZnO+1×WAT	585	95	0.162
1205×ZnO+1×WAT	1205	199	0.165
2410×ZnO+1×WAT	2410	393	0.163
4819×ZnO+1×WAT	4819	790	0.164
	Average GPC:		0.165

Table S3. Definitions of deposition schemes of ZnO, AZO-1, and AZO-2 ETL layers.

ETL layer	**Deposition scheme**	**Calculated thickness, nm**
ZnO	125×ZnO	20.6
AZO-1	5×(19×ZnO+1×AlO$_x$)+19×ZnO	18.7
AZO-2	6×(19×ZnO+1×AlO$_x$)	18.7

Table S4. The resistivity and Hall effect parameters of ZnO, AZO-1, and AZO-2 films.

Sample	Four-point probe method	Hall measurement		
	R (mΩ cm)	n (cm^{-1})	μ ($cm^2V^{-1}s^{-1}$)	R (mΩ cm)
ZnO	2260	$-(2.87\pm0.11)\times10^{18}$	1.25±0.05	1736.2±2.1
AZO-1	42.5	$-(7.85\pm0.41)\times10^{19}$	2.26±0.11	35.241±0.001
AZO-2	8.7	$-(1.40\pm0.10)\times10^{20}$	6.56±0.39	6.844±0.006

Table S5. Band energy values extracted from the UPS analysis in Figure S1.

Layer	E_g	E_v-E_f	E_f	E_v	E_c
ZnO	3.2	3.44	4.05	7.49	4.29
AZO-1	3.28	3.32	4.16	7.48	4.2
AZO-2	3.32	3.36	4.11	7.47	4.15

Note to Table S5: We note that the Fermi levels of all investigated ETLs are above their conduction bands. The reason for this phenomenon is doping level of the ETL as previously reported in the literature.[1-3] According to Burstein–Moss effect, once the dopant concentration in ETL is increased more than a certain limit, the concentration of charge carriers is increased. Thus, the Fermi level which normally is below the conduction band of ETLs is fully filled. Therefore, the extra excited electrons enter into the conduction band and we may observe such a phenomenon.

Table S6. XPS elemental analysis of ZnO, AZO-1, and AZO-2 films.

	ZnO		AZO-1		AZO-2	
	Peak Position eV BE	*Atomic Concentration (%)*	*Peak Position eV BE*	*Atomic Concentration (%)*	*Peak Position eV BE*	*Atomic Concentration (%)*
Zinc	1021.51	56.44	1021.76	45.32	1021.63	39
Aluminum	-	-	74.38	8.81	74.33	12.17
Oxygen O1s A	530.28	35.64	530.52	34.82	530.38	34.88
Oxygen O1s B	531.45	7.92	531.44	11.05	531.34	13.96

Table S7. Fitted results of TRPL curve of the various ETL/perovskite films.

Film	**τ_1 (ns)**	**A_1 (%)**	**τ_2 (ns)**	**A_2 (%)**	**$\tau_{ave.}$ (ns)**
Quartz/perovskite	34.3	0.15	155.8	0.85	151.3
ZnO/perovskite	12.9	0.19	60.2	0.81	57.9
AZO-1/perovskite	10.6	0.23	37.6	0.77	35.5
AZO-2/perovskite	5.4	0.36	29.5	0.64	27.3

The decay lifetime, τ, is estimated using the equation:

$$I(t) = I_0 + A_1 \exp\left(-\frac{t-t_0}{\tau_1}\right) + A_2 \exp(-\frac{t-t_0}{\tau_2}),$$

where $\tau_1$and τ_2 are first and second-order decay times and A_1 and A_2 are respective weight factors of each decay area.

Table S8. Parameters employed for the fitting of the impedance spectra of devices based on different ETLs.

Device	**R_s (Ω)**	**R_{ct} (Ω)**	**R_{rec} (Ω)**
ZnO	23.22	471.29	111.44
AZO-1	20.24	311.71	123.15
AZO-2	19.92	295.14	163.20

References:

[1] J. Jia, A. Takasaki, N. Oka, Y. Shigesato, *J. Appl. Phys*. **2012**, *112*, 013718.

[2] A. Saboor, S. M. Shah, H. Hussain *Mat. Sci. Semicon. Proc.* **2019**, *93*, 215-225.

[3] A. Klein, C. Körber, A. Wachau, F. Säuberlich, Y. Gassenbauer, S. P. Harvey, D. E. Proffit, T. O. Mason, *Materials* **2010**, *3*, 4892-4914.